Volume 7 | Number 4 | 21 February 2020

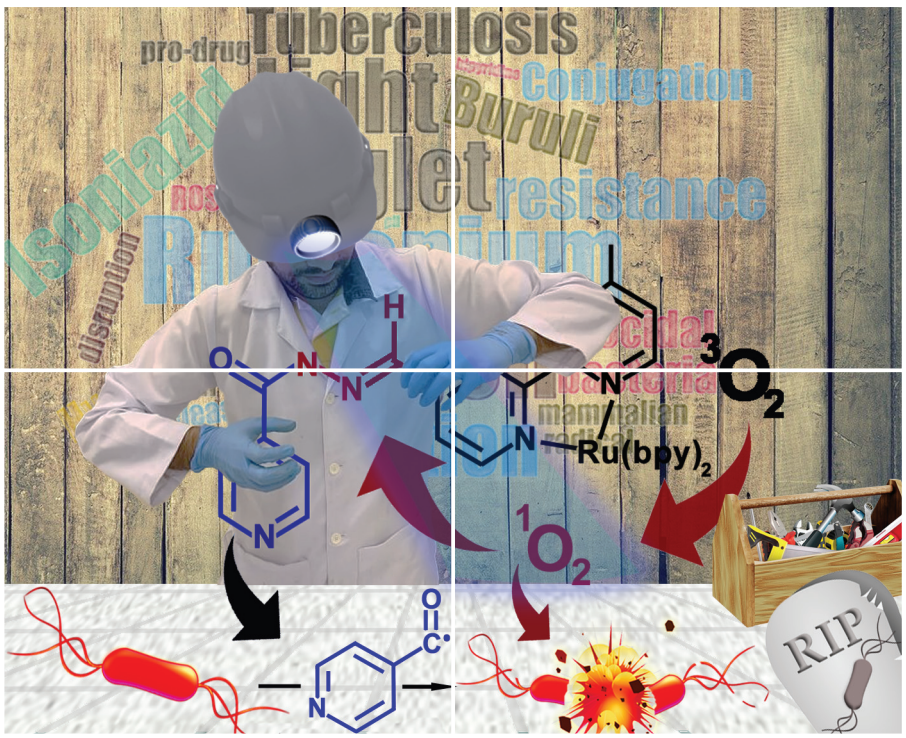

INORGANIC CHEMISTRY

FRONTIERS

CCS 中国化学会 CHINESE CHEMICAL SOCIETY
PEKING UNIVERSITY 1898
ROYAL SOCIETY OF CHEMISTRY
rsc.li/frontiers-inorganic

INORGANIC CHEMISTRY
FRONTIERS

RESEARCH ARTICLE

View Article Online
View Journal | View Issue

Cite this: *Inorg. Chem. Front.*, 2020, **7**, 859

Light-induced disruption of an acyl hydrazone link as a novel strategy for drug release and activation: isoniazid as a proof-of-concept case†

Edinaira Deodato Nunes,[a] Anne Drumond Villela,[b,c] Luiz Augusto Basso,[b,c] Edson H. Teixeira,[d] Alexandre L. Andrade,[d] Mayron A. Vasconcelos,[d,e] Luiz G. do Nascimento Neto,[d,f] Ana C. S. Gondim,[a] Izaura C. N. Diógenes,[a] Adolfo I. B. Romo,[a] Otaciro R. Nascimento,[g] Davila Zampieri,[h] Tércio Freitas Paulo,[a] Idalina Maria Moreira de Carvalho,[a] Luiz Gonzaga de França Lopes[a,b] and Eduardo H. S. Sousa[*a,b]

Received 12th September 2019,
Accepted 15th November 2019

DOI: 10.1039/c9qi01172b

rsc.li/frontiers-inorganic

Aldehydes and acyl hydrazines have been employed in a conjugation reaction that produces an acyl hydrazone bridge. A drawback to this linkage is hydrolysis, which prevents its broader use in a controllable manner. We have developed a new strategy for the cleavage of this group using a ruthenium(II) metal complex as a photogenerator of singlet oxygen. Isoniazid, an anti-tuberculosis prodrug, was chosen as a proof-of-concept compound; in this case it was coupled to an aldehyde-derivative trisbipyridine ruthenium(II) metal complex. Studies carried out using HPLC, MS, EPR, fluorescence and UV-vis showed that light could efficiently disrupt the acyl hydrazone linkage with the production of an isonicotinoyl radical. In addition, biological studies showed that bacterial strains and cancer cells became susceptible upon light irradiation. These results support a novel strategy of photoactivation based on a ruthenium metal complex conjugated to a pro-drug through an acyl hydrazone linkage, opening a broad range of applications.

Introduction

During the last decades, the number of tuberculosis (TB) cases has increased worldwide, particularly those caused by multi- and extensively drug-resistant strains.[1] This global threat has motivated several initiatives and the production of new anti-tuberculosis drugs, namely bedaquiline (2012) and delamanid (2013).[2] The scope of these drugs is limited to their use as a third-line treatment against *Mycobacterium tuberculosis* (Mtb), the major causative agent of TB. The shortage of efficient drugs against other mycobacterial infections (*e.g. Mycobacterium leprae* and *Mycobacterium ulcerans*) is even more remarkable. This has stimulated the search for new drugs.

The current tuberculosis treatment uses a cocktail of drugs that were approved during the 1950s and 1960s. Several of these anti-TB agents are prodrugs such as isoniazid, pyrazinamide, ethionamide, and *p*-aminosalicylic acid, including the most recently approved delamanid.[2] Interestingly, in clinically-isolated Mtb strains, the most recurrent mechanism of resistance relies on the disruption of the routes of biological activation of these prodrugs.[2] Since 1952, isoniazid has been a frontline prodrug in clinical use, but its use has suffered from a large number of resistant strains of Mtb and unpleasant side effects.[2] In particular, about 50% of the isoniazid-resistant clinical Mtb isolates have showed deletions or mutations in the catalase-peroxidase enzyme, KatG, that is responsible for the activation of isoniazid.[3,4] This activation process is an oxidative reaction catalyzed by KatG, which can be mimicked by manganese(III) complexes and others.[5–7] Attempts to oxidize

[a]*Laboratório de Bioinorgânica, Departamento de Química Orgânica e Inorgânica, Universidade Federal do Ceará, CEP 60455-760 Fortaleza, Ceará, Brazil. E-mail: eduardohss@dqoi.ufc.br*
[b]*Instituto Nacional de Ciência e Tecnologia em Tuberculose, Pontifícia Universidade Católica do Rio Grande do Sul, Porto Alegre, Brazil*
[c]*Pontifícia Universidade Católica do Rio Grande do Sul, Centro de Pesquisas em Biologia Molecular e Funcional, Av Ipiranga 6681, Porto Alegre, RS 90619-900, Brazil*
[d]*Laboratório Integrado de Biomoléculas, Departamento de Patologia e Medicina Legal, Universidade Federal do Ceará, 60441-750 Fortaleza, Ceará, Brazil*
[e]*Departamento de Ciências Biológicas, Faculdade de Ciências Exatas e Naturais, Universidade do Estado do Rio Grande do Norte, 5625-620 Mossoró, Rio Grande do Norte, Brazil*
[f]*Federal Institute of Education, Science and Technology of Ceara (IFCE), postal code 62930-000, Limoeiro do Norte-Ceará, Brazil*
[g]*Departamento de Física Interdisciplinar, Instituto de Física de São Carlos, Universidade de São Paulo, 13560-970 São Carlos, São Paulo, Brazil*
[h]*Biotechnology and Mass Spectrometry Research Group, Federal University of Ceará, 60440-900 Fortaleza, Ceará, Brazil*

†Electronic supplementary information (ESI) available. See DOI: 10.1039/c9qi01172b

isoniazid directly with hydrogen peroxide, for example, have had marginal success.[8]

Among the new strategies for drug development, those using metal complexes have stood out due to innovative proposals and promising biological results.[9–14] A new approach for tuberculosis drug treatment was developed in our lab by modifying isoniazid using an iron moiety (pentacyanoferrate(II)).[15] This new compound, known as IQG607, had the ability to generate activated isoniazid without enzymatic processing.[5,8] This finding has motivated further chemical[6,8,16,17] and biological studies.[18–22] Indeed, stoichiometric amounts of hydrogen peroxide fully oxidized isoniazid bound to iron within a few minutes; such an oxidation cannot be achieved with free isoniazid even after 6 hours.[8] A series of studies have supported that a non-Fenton reaction takes place, where most likely an intramolecular electron transfer process of activation occurs.[5,6,17] The biological mechanism of action of IQG607, however, might not be through a redox-mediated activation, as originally proposed.[5,23] Nonetheless, this metal compound has shown great anti-tuberculosis activity, with a favorable toxicological profile compared to free isoniazid, and it has been increasingly used in pre-clinical trials.[20–23]

Ruthenium complexes containing isoniazid have also been prepared and have shown potential anti-mycobacterium activity.[24–26] The photorelease of isoniazid has been pursued as a new uncaging strategy, using either bipyridine-based[24] or terpyridine-based[25] ruthenium complexes, giving promising results. These complexes, however, did not tackle the activation step: an important issue that is at the core of isoniazid resistance. Therefore photo-uncaged isoniazid would still be subject to resistance by Mtb strains with mutated KatG. To address this key issue, a proof-of-concept compound was prepared by coupling a trisbipyridine-like ruthenium(II) complex with isoniazid conjugated through an acyl hydrazone linkage, aiming to release activated isoniazid under blue-light irradiation (Fig. 1). The acyl hydrazone linkage has been widely used, but it has drawbacks, particularly due to hydrolysis, while light has only promoted photoisomerization.[27,28] Here, we show evidence that the use of light coupled to a ruthenium(II) complex can selectively disrupt this acyl hydrazone group. This novel approach may be broadly used to photorelease and activate many other biologically active species.

Experiment

Materials

All reagents such as isoniazid, 4,4′-dimethyl-2,2′-bipyridine, sodium azide, tris-HCl, superoxide dismutase (SOD), catalase, D-mannitol, selenium dioxide, 1-hydroxybenzotriazole hydrate (HOBT), *N*-methylmorpholine (NMM), ruthenium(II) trisbipyridine chloride (**Ru-bpy**), and tetrabutylammonium perchlorate (PTBA) from Sigma-Aldrich-Merck, acetonitrile, methanol (MeOH) HPLC grade from Tedia (Brazil), ruthenium(III) chloride hydrate from Precious Metals Online (PMO, Australia) Pty Ltd, and sulfuric acid and trifluoracetic acid (HTFA) from Merck were of analytical grade and were all used as received. Acetone (Mallinckrodt) was treated with sodium sulfate and then distilled and stored over 4 Å molecular sieves. Precursor *cis*-$[Ru(bpy)_2(mbpy\text{-}COH)](PF_6)_2$ (**Ru-CHO**), where bpy = 2,2′-bipyridine and mbpy-COH = 4′-methyl-2,2′-bipyridine-4-carboxaldehyde, was prepared as reported elsewhere (elemental analysis, experimental (theoretical): C, 42.76 (42.63); H, 2.89 (2.91); N, 9.24 (9.32); FTIR (KBr pellet): νC=O, 1708 cm^{-1}; $E_{1/2}$ (0.1 mol L^{-1} PTBA, *vs.* Ag|AgCl) 1.357 V, HRMS (*m*/*z*): theoretical 306.061 and found 306.061 $[M]^{2+}$ and theoretical 322.074 and found 322.075 $[M + MeOH]^{2+}$; ^{1}H-NMR (dimethyl-

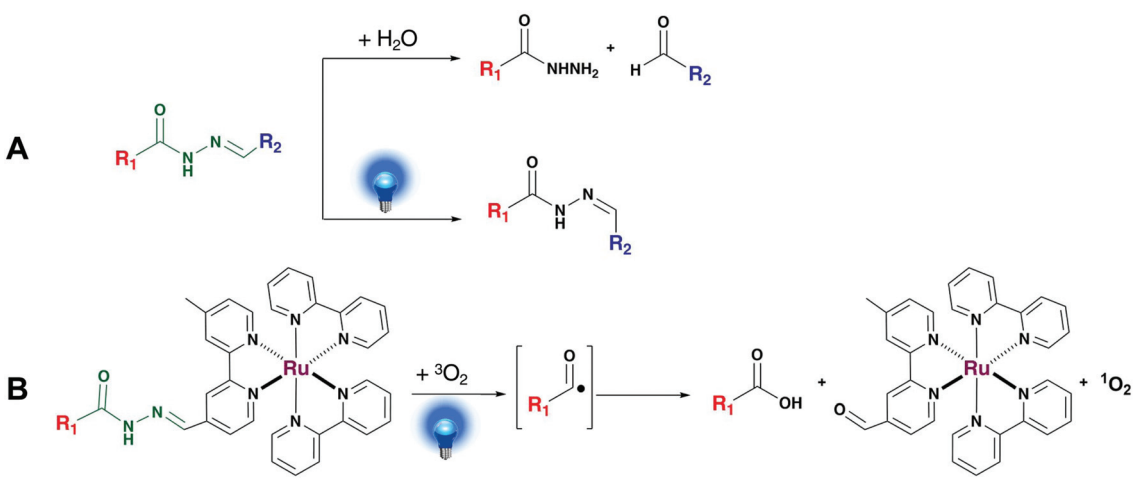

Fig. 1 Chemistry of the acyl-hydrazone conjugation group. In panel A, we show the common changes reported for this group, either hydrolytic disruption or photoisomerization. In panel B, we show a new strategy for the controlled cleavage of acyl hydrazone by coupling to a singlet-oxygen-generator species (*e.g.* trisbipyridine ruthenium(II)). Once this highly reactive species is produced with light, it disrupts the acyl hydrazone linkage. If R_1 is the 4-pyridyl group coupled to a ruthenium metal complex, then this compound (**Ru-INH**) might be able to give an isonicotinoyl radical intermediate, which is the activated form of the pro-drug isoniazid, which further decays into isonicotinic acid.

sulfoxide-d6, 300 MHz): δ = 10.18 (s, 1H; CHO), 9.19 (s, 1H; m3), 8.96 (s, 1H; m3′), 8.86 (d, 4H; b3,3′), 8.20 (m, 4H, b4,4′), 8.06 (d, 1H, m6), 7.86 (d, 1H, m5), 7.79 (d, 1H, m6′), 7.74 (d, 4H, b6,6), 7.56 (m, 4H, b5,5′), 7.43 (d, 1H, m5′), 2.47 (s, 3H, CH_3), see ESI Fig. S1†).[29] Tryptic soy broth and tryptic soy agar media used in the antimicrobial assays were obtained from HiMedia (India). For cell culture conditions, phosphate buffered solution (PBS; pH 7.4), heat-inactivated fetal bovine serum (FBS), L-glutamine (200 mmol L^{-1}), trypsin/EDTA solution (TE) and penicillin–streptomycin were purchased from Gibco® (Thermo Fisher Scientific, USA). Roswell Park Memorial Institute 1640 medium (RPMI 1640) and Dulbelcco's modified Eagle's medium (DMEM) were purchased from GE-Hyclone® (USA). CellTiter 96® aqueous MTS reagent powder ([3-(4,5-dimethylthiazol-2-yl)-5-(3-carboxymethoxyphenyl)-2-(4-sulfophenyl)-2*H*-tetrazolium]) was purchased from Promega Inc (USA).

Synthesis of *cis*-[Ru(bpy)$_2$(mbpy-INH)](PF$_6$)$_2$ (Ru-INH)

50 mg (0.055 mmol) of the precursor metal complex *cis*-[Ru(bpy)$_2$(mbpy-COH)](PF$_6$)$_2$ (**Ru-CHO**) and 23 mg (0.17 mmol) of isoniazid (**INH**) were mixed in 40 mL of ethanol : water (1 : 1). This mixture was kept under argon, light protected and refluxed for 7 h. Subsequently, a saturated solution of NH_4PF_6 was added and a solid was collected and dried (49 mg, 0.048 mmol, yield 86%). Elemental analysis, experimental (theoretical): C, 45.38 (45.04); H, 3.49 (3.50); N, 11.77 (11.82); ^{1}H-NMR (acetone-D6, 300 MHz): δ = 11.92 (s, 1H; i6), 9.18 (s, 1H; m3), 8.90 (s, 1H; m3′), 8.81 (d, J = 8.4 Hz, 5H; b3, i2), 8.64 (s, 1H; i7), 8.22 (t, 4H; b4), 8.15 (m, 1H; m6), 8.05 (d, J = 8.4 Hz, 4H; b6), 7.91–7.71 (m, 4H; m5, m6′ and i3), 7.58 (m, 4H; b5), 7.44 (d, J = 5.8 Hz, 2H; m5′), 2.60 (s, 3H, 4′-CH_3) (see ESI Fig. S2†); ^{13}C-NMR (acetone-D6, 100.63 MHz): δ = 159.00 (Ci5), 158.23 (Cb2), 157.48 (Ci4), 152.79 (Cm2), 152.68 (Cb6), 151.85 (Ci2), 151.68 (Cm4′), 145.36 (Ci7), 144.45 (Ci3), 139.04 (Cb4), 129.87 (Cm5′), 128.87 (Cb5), 126.61 (Cm3′), 125.42 (Cb3, Cm5, Cm6′), 122.23 (Cm3, Cm6′), 21.25 (Cm4′-CH_3) (see ESI Fig. S3†); HRMS (m/z): theoretical 365.585 $[M]^{2+}$ and found 365.586 $[M]^{2+}$.

Measurements

NMR spectra were obtained using a Bruker AVANCE DPX 300 spectrometer (300 MHz), in deuterated DMSO. Absorption spectra of dilute solutions (*ca.* 5 × 10^{-5} mol L^{-1}) were measured using a spectrophotometer Cary 5000 model (Agilent), and steady-state emission spectra were recorded using a Quanta-Master QM-40 PTI-Horiba (exc. at 450 nm, slits at 1 mm). Electrochemical measurements were carried out using an Epsilon potentiostat (Bioanalytical Systems Inc. (BAS), West Lafayette, IN) at 25 ± 0.2 °C using a conventional three-electrode glass cell with glassy-carbon, platinum-wire, and Ag/AgCl (KCl 3.5 mol L-1, BAS) as working, auxiliary, and reference electrodes, respectively. All potentials reported in this work are referenced against Ag/AgCl, corrected using ferrocene. Based on the cyclic voltammetry techniques, the half-wave potentials ($E_{1/2}$) were calculated, when possible, by averaging the anodic and cathodic peak potentials.

Computational details

All density functional theory (DFT) calculations in this study were performed using the Gaussian 09 program package, revision A.02 (Gaussian Inc., Wallingford, CT).[30] The geometry of the metal complex was optimized at the DFT level by means of the B3LYP functional.[31–33] The 6-31G(d) basis set was used for C, H, O, and N atoms, and the LANL2DZ relativistic effective core potential basis set was used for the Ru atom. Optimized geometries in a minimum of the potential energy were confirmed by the absence of any imaginary frequency in vibrational analysis calculations. On the basis of the optimized geometries, time-dependent DFT (TD-DFT) was applied to investigate the electronic properties of the metal complexes and simulate the absorption spectra. TD-DFT calculations were carried out in methanol solvent fields by means of a polarizable continuum model.[34] The molecular orbital composition, UV–vis spectra, and assignment of principal transitions were extracted using Multiwfn[35] and GaussSum 3.0[36] programs, respectively.

Chromatographic experiments

All chromatographic measurements were conducted with C-18 reverse-phase columns purchased from Waters; for photoreactivity studies Sunfire column (250 mm × 4.6 mm, 5 μm particle size) was used while for monitoring syntheses, μBondapak (150 mm × 4.6, 10 μm particle size) was used. A gradient elution of acetonitrile and HTFA solution pH 3.5 was used for separation. All chromatographic experiments were performed using a Shimadzu liquid chromatography (HPLC) instrument equipped with a model LC-10 AD pump and a SPD-M20A UV-visible (UV–Vis) photodiode-array detector with a CBM-10 AD interface. Samples of 20 μL were injected along with standard solution to identify and quantify the products.

A series of 0.25 mmol L^{-1} of **Ru-INH** was prepared in aqueous solution, where pH was adjusted from 1 up to 13 using HCl or NaOH, and incubate for 15 h at 25 °C. After this, these samples were injected into the HPLC and compared to fresh standard solution. A liquid chromatography analytical process was developed in which an initial gradient was used from 20 to 50% acetonitrile (0 to 30 min) followed by a decrease from 50 to 20% acetonitrile (30 to 35 min) and an isocratic step at 20% acetonitrile (35 to 40 min). In addition to this, 1 mmol L^{-1} of **Ru-INH** in ethanol was also monitored by HPLC during blue LED irradiation (Basetech Conrand, 1.7 W). Another analytical liquid chromatographic strategy was developed in which initially an isocratic step of 10% methanol (0 to 7.5 min) followed by a gradient from 10 to 40% methanol (7.5 to 10.5 min) and a second isocratic step of 40% methanol (10.5 to 25 min), then back to 10% methanol (25 to 35 min) was employed for the latter.

Measurement of reactive oxygen species (ROS)

1,3-Diphenylisobenzofuran (DPBF) was chosen to measure the quantum yield of singlet oxygen ($^1O_2$) generation by ruthenium metal complexes. DPBF is a fluorescent probe that reacts selectively with $^1O_2$ to produce a non-fluorescent product. A series of 2 mL air-saturated ethanol solutions containing DPBF (20 μmol L^{-1}) and the ruthenium metal complexes were prepared in a 1 cm pathlength fluorescence cuvette and illuminated with LED light of 463 nm (Basetech Conrand, 1.7 W) for 100 seconds. The consumption of DPBF by reaction with $^1O_2$ was followed by fluorescence at the emission maximum (excitation λ_{ex} = 405 nm, emission λ_{em} = 479 nm) at different irradiation times. Aminophenyl fluorescein (APF) was used to measure the photogeneration of the hydroxyl radical (HO$^\bullet$) by monitoring the increase of an emission band at 515 nm. A quartz cuvette containing 600 μL of the metal complexes (10 μmol L^{-1}) in 0.1 mol L^{-1} in PBS (pH 7.4) was irradiated with LED light of 463 nm (Basetech Conrad, 1.7 W) in the presence of APF (5 μmol L^{-1}). Additional controls were prepared to further validate singlet oxygen contribution to this reaction using sodium azide and D-mannitol as $^1O_2$ and hydroxyl scavenger agents, respectively.

Fluorescence study of the effect of oxygen and hydrogen peroxide

Two samples of 50 μmol L^{-1} of **Ru-INH** were prepared in aerated and deaerated ethanol, which were irradiated with blue LED (max. at 463 nm, 20 W) and their fluorescence spectra were recorded (λ_{ex} = 450 nm, slits at 1 mm). Additionally, a sample of 50 μmol L^{-1} of **Ru-INH** in ethanol was mixed with hydrogen peroxide and monitored by fluorescence.

Electron paramagnetic resonance (EPR)

EPR spectra of the isoniazid conjugated ruthenium metal complex (5 mmol L^{-1}) were recorded in acetonitrile solution, containing 50 mmol L^{-1} of the spin trap *N-tert*-butyl-α-phenylnitrone (PBN). They were acquired at 25 °C using a Varian E-109 X-band instrument with a standard rectangular cavity using a glass quartz flat cell (Wilmad) under blue-light (463 nm) irradiation for 20 h. Measurement conditions were: center field, 339 mT; sweep field, 10 mT; sweep time, 60 s; MW power, 20 mW; gain, 2.0 × 10^3, modulation amplitude, 0.05 mT; modulation frequency, 100 kHz; time constant, 0.064 s; and MW frequency, 9.50390 GHz. Spectral simulations were prepared using the EasySpin program[37] with the following EPR parameters for PBN: g = 2.0063, line width = 0.149 mT, A^N = 1.638 mT, A^H = 0.318 mT.

Mass spectrometry

The determination of the molecular mass of the compounds was performed using an HPLC system (Agilent 1290 Infinity LC System) consisting of a degasser, two binary pumps and a thermostat (4 °C) auto-coupled with a Q-ToF-MS mass spectrometer (6550 iFunnel, Agilent Technologies). The mass spectra of the components were obtained by ionization by ESI in positive ion mode, with the following parameters: centroid mode at a rate of 1.0 spectrum per second (2 GHz). The capillary voltage was set to +3.5 kV; the N_2 drying gas flow rate was 6 L min^{-1} at 300 °C and the nebulizer gas was at 30 psi. The continuous internal calibration was performed during the analysis by the automatic calibration system using a calibration solution, comprising reference mass m/z 922.0097 (HP-0921, hexaquis (1H, 1H, 3H tetrafluoropropoxyphosphazine). Data acquisition was performed over the range of m/z 100–1200. All samples were diluted in methanol and, whenever mentioned, blue-light irradiated.

DNA cleavage assays

The cleavage studies with DNA were carried out using commercial pBR322 plasmid (NEB, USA) at 100 ng per well. The following compounds were used in these experiments: **Ru-CHO**, **Ru-INH** and **Ru-bpy** along with free isoniazid (**INH**). Each of them was incubated for 1 h with the DNA in the dark or upon blue-light irradiation (LED at 463 nm, 5 × 4.5 cm, 1.7 W) in Tris buffer (pH 8.0). The concentration of **Ru-INH** was varied from 5 μmol L^{-1} to 50 μmol L^{-1}, while those of the controls **Ru-CHO**, **INH** and **Ru-bpy** were kept constant at 50, 50 and 20 μmol L^{-1}, respectively, along with a standard linear 1-Kb DNA ladder (NEB, USA). Another protocol to investigate the species involved in the cleavage was performed as follows: 1 h of blue-light irradiation of a Tris buffer (pH 8.0) containing 10 μmol L^{-1} of **Ru-INH** and sodium azide (20 mmol L^{-1}), mannitol (20 mmol L^{-1}), superoxide dismutase (SOD, 20 U mL^{-1}) and catalase (20 U mL^{-1}) as selective scavengers for the reactive oxygen species $^1O_2$, HO$^\bullet$, O_2^- and H_2O_2, respectively. All samples were run in 0.8% (w/v) agarose gel for about 30 minutes and stained with GelRed (Biotium, USA), and images of the gel were collected and analyzed using a Gel DocTM XR + System (Biorad).

Biological assays

Microorganisms and culture conditions. The bacteria used in this study included *Staphylococcus aureus* ATCC (American Type Culture Collection) 25923, *Staphylococcus epidermidis* ATCC 12228, *Pseudomonas aeruginosa* ATCC 10145, *Escherichia coli* ATCC 11303, *Mycobacterium tuberculosis* (H37Rv) and *M. tuberculosis* (MDR, CDCT-16). These strains were stored in tryptic soy broth (TSB) with 20% (v/v) glycerol at −80 °C. They were inoculated in tryptic soy agar (TSA) plates and incubated aerobically at 37 °C for 24 h. After growing on agar plates, individual colonies were removed and inoculated in a 10 mL of a fresh TSB medium and incubated for 24 h at 37 °C under steady agitation. Prior to each antibacterial assay, the final cell concentration was adjusted to 1 × 10^6 colony-forming units (cfu) mL^{-1}.

Antibacterial assay. The susceptibility of the bacteria to the ruthenium metal complexes and free isoniazid was evaluated from the minimum inhibitory concentration (MIC) and minimum bactericidal concentration (MBC) of the compounds. The MIC values were determined according to the National Committee for Clinical Laboratory Standards M7-A6 (NCCLS, 2003), with minor modifications. Briefly, the compounds were diluted in ultrapure sterile water at concen-

trations ranging from 3.9 to 250 μg mL^{-1} and dispensed into 96-well plates, each of which had a bacterial suspension (1×10^6 cfu mL^{-1}) in TSB. These plates were subjected to irradiation with blue LED (463 nm, 425 mW cm^{-2}) for 1 h or kept in the dark and then incubated overnight at 37 °C. The MIC was defined as the lowest compound concentration that completely inhibited visible bacterial growth. For the measurements of MBC, 10 μL was removed from each well, where no visible bacterial growth was observed, plated onto TSA plates, and incubated at 37 °C. The MBC was considered to be the lowest compound concentration for which colony growth was not observed.

Cell lines and culture conditions. Human breast adenocarcinoma (MCF-7; HTB-22®), prostate carcinoma (LNCAP clone FGC), human lung adenocarcinoma (A549; CCL-185®) and murine fibroblast (NCTC-CL929) cell lines from ATCC® (American Type Culture Collection, EUA) were purchased from the bank of cells of Rio de Janeiro (BCRJ). The cells were maintained in T-25 flasks containing DMEM medium (L929 and A549) or RPMI medium (MCF-7 and LNCAP) both supplemented with 10% fetal bovine serum (FBS), 1% L-glutamine, 100 U ml^{-1} penicillin and 100 μg ml^{-1} streptomycin, at 37 °C, under a humidified atmosphere containing 5% CO_2. The culture medium was routinely changed every three days or when *ca.* 90% confluence was reached; then the cells were treated with trypsin (0.025% trypsin/0.1% EDTA) and subcultivated or used for viability assays. In all assays the cells were used between passage numbers 3 and 10.

Cell viability assay. To determine the effect of the ruthenium metal complexes on cell viability, we used the CellTiter 96 Aqueous MTS reagent powder (Promega), according to the manufacturer's instructions. After trypsinization with TE, the cells (1.0×10^4 per 200 μl per well) were seeded into 96-well flat bottom plates in DMEM or RPMI containing 10% FBS and incubated overnight. After this, the supernatant was removed and replaced by fresh culture medium (DMEM or RPMI) containing different concentrations of the ruthenium metal complexes or free isoniazid. Subsequently, these plates were subjected to irradiation with blue LED (463 nm, 425 mW cm^{-2}) for 1 h or kept in the dark and then incubated overnight at 37 °C. Cell viability assays using MTS salt were performed at 48 h for all cell lines. Therefore, all culture medium was removed and replaced with non-supplemented medium (DMEM or RPMI) containing MTS tetrazolium salt. The optical density was measured at 490 nm on a microplate reader (SpectraMax i3). All assays were carried out in triplicate, for three independent experiments, where cell viability was calculated using the equation given below. In addition to this, controls of cells without metal complexes and irradiated with blue light and also controls of cells without light irradiation were prepared.

$$\text{Cell viability}(\%) = (\text{Abs, average OD at 490 nm(compounds)})/(\text{Abs, average OD at 490 nm(cell control)}) \times 100$$

Statistical analysis. The data obtained in the cell viability assay are presented as mean ± SEM. Experimental data were assessed by using Student's *t*-test. $P < 0.001$ (***) and $P < 0.05$ (*) were considered as the level of significance. The values were calculated using the software GraphPad Prism® 5.

Results and discussion

Characterization of the isoniazid-conjugated ruthenium metal complex (Ru-INH)

The synthesis of **Ru-INH** was monitored by HPLC using a C18 reverse-phase column. In the beginning, only two peaks were observed, with electronic spectra consistent with those of isoniazid (**INH**) (retention time (t_R) = 2.2 min) and the precursor aldehyde-bipyridine ruthenium(II) metal complex (**Ru-CHO**) (t_R = 9.8 min). After 7 hours, none of the precursor ruthenium metal complex could be observed, and a major new peak appeared (t_R = 13.4 min) as indicated by HPLC (ESI Fig. S4†). After isolation, this new metal complex was re-injected into the HPLC, wherein a single peak was observed (t_R = 13.4 min) indicating a high level of purity. ^{1}H-NMR analysis supported its production through an efficient coupling reaction of the precursor aldehyde-based ruthenium(II) trisbipyridine (**Ru-CHO**), where the aldehyde group disappeared while the number of hydrogens increases in agreement with the conjugation (ESI Fig. S1–S3†). Additionally, elemental analysis was fully consistent with the formulation proposed, along with a high-resolution mass spectrum obtained using a qTOF mass spectrometer (theoretical 365.5848 $[M]^{2+}$; experimental 365.5862 $[M]^{2+}$) (ESI Fig. S5†). Mass spectrometry was also employed to monitor the formation of the ruthenium metal complex, in which even after 1 h of reaction at room temperature, it was possible to observe the appearance of a signal with mass at 365.5862, corresponding to **Ru-INH**. Infrared spectroscopy measurements showed that the band assigned to the carbonyl stretching vibration mode of the aldehyde group, observed at 1708 cm^{-1} in the spectrum of **Ru-CHO**, disappeared while a new one was observed at 1685 cm^{-1}, which is assigned to the C=O stretching mode of the acyl hydrazone group. Additionally, the N–H stretching mode associated with the acyl hydrazone moiety was observed at 3336 cm^{-1}, supporting the attachment of this fragment to the metal complex through the bipyridine moiety (ESI Fig. S6†). The electronic spectrum of **Ru-INH** showed typical intraligand bands along with a shoulder at *ca.* 340 nm, which was only observed after conjugation with isoniazid, likely due to the acyl hydrazone moiety (ESI Fig. S7†).[38] Furthermore, an electronic absorption transition band assigned to a metal-to-ligand-charge transfer (MLCT) transition was observed with a modest blue shift from 452 nm in **Ru-CHO** to 461 nm in **Ru-INH**. TD-DFT calculations indicated that the lower-energy electronic absorption of **Ru-INH** arises from the transitions of the highest-occupied molecular orbital−1 (HOMO−1) to the lowest-unoccupied molecular orbital (LUMO) and HOMO−2 to LUMO+1 at 440 and 411 nm, respectively. The HOMO−1 and HOMO−2 are centered mainly on the metal while the LUMO and LUMO+1 are centered on mbpy-INH and bpy ligands, respectively (Fig. 2). These results

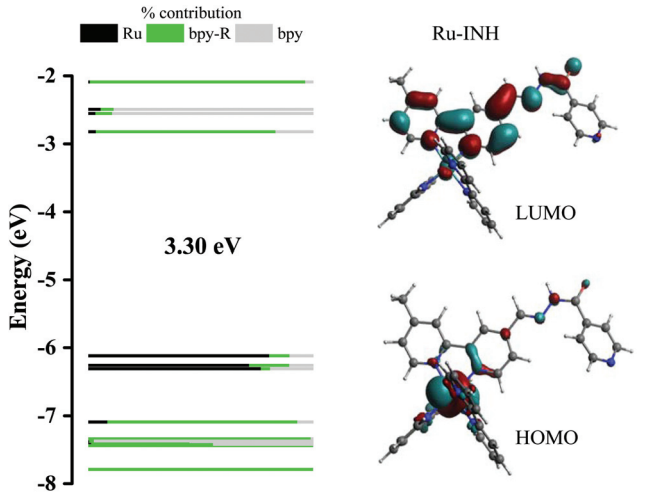

Fig. 2 Energy level diagram and percent contribution in the frontier molecular orbitals of the metal complex **Ru-INH**. Inset: Isodensity plots, with 0.03 isovalues of the HOMO and LUMO in **Ru-INH**. (bpy-R = mbpy-INH).

reinforce the MLCT character of this band in the visible region. More detailed transition data of the **Ru-INH** metal complex are provided in ESI Table S1.† Interestingly, the electron density mappings of the frontier orbitals indicated a major LUMO contribution for the acyl hydrazone bipyridine moiety, making it susceptible to oxidative attack upon excitation (Fig. 2).

Electrochemical measurements were carried out using 0.1 mol L^{-1} tetrabutylammonium perchlorate in acetonitrile and scanning from −2.0 to 2.0 V with a glassy carbon electrode *vs.* Ag|AgCl. A set of waves was observed for the **Ru-CHO** precursor with bipyridine reductive processes observed at −1.726, −1.500 and −1.305 V, while $E_{1/2}$ for $Ru^{3+/2+}$ was shown at +1.357 V (ESI Fig. S8†). For **Ru-INH**, besides the reductive waves of bipyridines observed at −1.750, −1.480 and −1.281 V, another reductive wave at −0.430 V was observed along with $E_{1/2}$ for $Ru^{3+/2+}$ at +1.365 V (ESI Fig. S8†). This new reductive wave seems to be consistent with the isoniazid moiety, which, as a free species, showed a redox process at *ca.* −0.540 V under these conditions. Nonetheless, electrochemistry measurements for this metal complex indicated minor changes in the electrochemical potentials. These small changes observed for the Ru(III/II) redox potentials are consistent with the spectroscopic results for the optical MLCT transition. The high electrochemical potential found for the **Ru-INH** metal complex makes it unlikely that any oxidation of the ruthenium would occur within cells, supporting its integrity.

Chemical and photochemical reactivity

To investigate the chemical stability of the acyl hydrazone linkage used in the isoniazid-conjugated ruthenium(II) metal complex, we kept this compound in aqueous solutions with pH values ranging from 1 to 13, for 15 h at 25 °C, in the dark. Subsequently, all the samples were injected into a HPLC and their chromatograms were recorded (ESI Fig. S9†). In most of the chromatograms only one peak, corresponding to the original ruthenium metal complex, **Ru-INH**, was observed. At pH values 1 and 2, new chromatographic peaks were detected, indicating decomposition of *ca.* 51 and 14% of **Ru-INH**, respectively, while at pH 3 higher decomposition of less than 6.5% was noticed after 15 hours (ESI Fig. S9†). These results indicate that **Ru-INH** may withstand acidic and basic conditions. This feature makes this compound likely to be suitable for oral administration as well. However, beyond pH stability, it remains to be shown that it is well absorbed, which also depends on the lipophilicity of the compound. In addition to this, acyl hydrazones are usually more stable toward hydrolysis than imines,[39] making this bridge quite appropriate.

To investigate the photostability of **Ru-INH**, it was irradiated with blue light (LED source, 463 nm, 1.7 W) for 5 h at 25 °C and monitored by HPLC, absorption, and emission spectroscopy. During light irradiation, a slight blue shift of the MLCT band (from 461 nm to 456 nm) was observed in the electronic spectra along with an increase in the absorbance (ESI Fig. S10†). We noticed that the final spectrum was similar to that of **Ru-CHO**, suggesting that it could be regenerated upon light irradiation.

Luminescence measurements of the **Ru-INH** metal complex showed maximum emission at 608 nm in ethanol, while the ruthenium precursor, **Ru-CHO**, emitted at 598 nm under identical conditions. The energy of the ^{3}MLCT state of **Ru-INH** stabilized in about 0.4 kcal mol^{-1} when compared to the energy of the E_{00} transition of the precursor metal complex. During light irradiation, the **Ru-INH** metal complex showed a gradual increase in luminescence intensity as well as a blue shift of the band toward 598 nm, which was also similar to that observed for **Ru-CHO** (ESI Fig. S10†). This measurement is in agreement with the electronic absorption spectroscopy results, also indicating the formation of the ruthenium precursor, **Ru-CHO**, after photolysis.

The chromatograms obtained during the blue-light irradiation of **Ru-INH** (Fig. 3) showed major changes, particularly a gradual decrease in its peak (1, t_R = 23.1 min), and the appearance of two new peaks (2, t_R = 4.7 min and 3, t_R = 17.0 min), whose intensities reached a plateau after *ca.* 5 h (Fig. 3). The electronic spectra corresponding to peaks 1, 2 and 3 shown in Panel B of Fig. 3 are consistent with the formation of a ruthenium-based compound (peak 2) and a free pyridinic-based ligand (peak 3). The following standard compounds were injected into the HPLC (same conditions as shown in Fig. 3) to validate the identity of the generated species: isonicotinic acid (t_R = 4.70 min), isoniazid (t_R = 7.36 min), isonicotinamide (t_R = 9.10 min) and **Ru-CHO** (t_R = 17.0 min). Based on those measurements, peaks 2 and 3 were assigned to **Ru-CHO** and isonicotinic acid, respectively. High-resolution mass spectrometry was also used to monitor this photochemical reaction, where a mass consistent with the ruthenium precursor (**Ru-CHO**) was found, supporting its photoproduction (ESI Fig. S11†). In addition to **Ru-CHO**, mass spectrometry showed a hemiacetal derivative of **Ru-CHO** (ESI Fig. S11†) that can emerge from a methanolic solution, and a carboxylic ruthenium

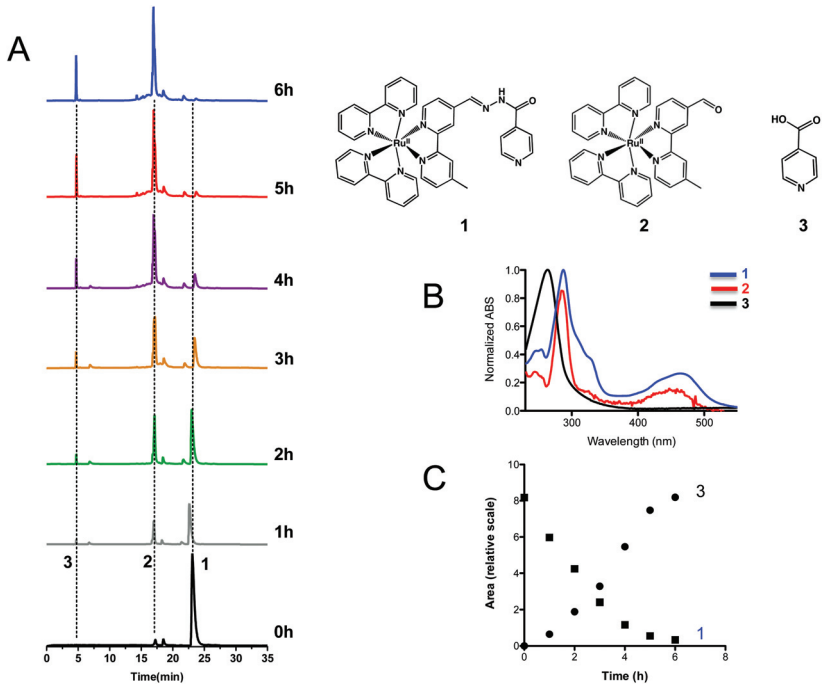

Fig. 3 Products of blue-light irradiated **Ru-INH**, as monitored by chromatography. Panel A shows a set of chromatograms of **Ru-INH** during 6 h of blue-light irradiation, while panel B shows the spectra for peaks 1, 2 and 3 obtained in the HPLC. Panel C shows the change of the peak area over time for peaks 1 and 3, assigned to **Ru-INH** and isonicotinic acid, respectively.

species, whose formation is shown in ESI Fig. S11.† A mechanistic proposal for the photoactivation process of **Ru-INH** has been drawn (ESI Fig. S13†). As far as we know, this is the first time that an acyl hydrazone linkage has been photochemically disrupted, opening a broad range of applications. Light irradiation of this functional group has usually been reported to promote only photoisomerization (see Fig. 1).[27,28,40]

The production of isonicotinic acid upon blue-light irradiation of **Ru-INH** is an important evidence for the activation of isoniazid. As a matter of fact, isoniazid is mainly converted to its acid form, once activated by the catalase-peroxidase KatG enzyme or during mimicking activation using Mn(III) metal complexes as well.[2,41]

Photochemical production of reactive oxygen species

The only trigger used here for the production of isonicotinic acid was blue light, which might have produced reactive species leading to the disruption of the acyl hydrazone linkage. Since $[Ru(bpy)_3]^{2+}$ (**Ru-bpy**) is a well-known photogenerator of ROS (reactive oxygen species),[42] a further investigation of this issue was performed for **Ru-INH** using DPBF (1,3-diphenylisobenzofuran) and APF (aminophenyl fluorescein) as probes for singlet oxygen and hydroxyl radicals, respectively. ESI Fig. S14† shows the fluorescence spectra of **Ru-INH**, **Ru-CHO**, and **Ru-bpy** in the presence of the probes.

The values of oxygen singlet quantum yield (Φ_Δ) were calculated based on the rate constants (ESI Fig. S14B†), using the standard **Ru-bpy** ($[Ru(bpy)_3]^{2+}$, $\Phi_\Delta = 0.84$[43]). As can be ascertained from ESI Fig. S14,† **Ru-INH** showed low production of $^1O_2$ ($\Phi_\Delta = 0.23$) using DPBF, even lower than **Ru-CHO** ($\Phi_\Delta = 0.46$). This result might be interpreted as a competing reaction of consumption of the $^1O_2$, which may react with the DPBF probe as well as disrupting the acyl hydrazone linkage. The measurement using APF in the presence of sodium azide and D-mannitol supports that a hydroxyl species is not significantly produced, while singlet oxygen is the main photogenerated product (ESI Fig. S14†). These results mainly support the formation of $^1O_2$, which may be responsible for the cleavage of the acyl hydrazone linkage and isoniazid activation.

In addition to these measurements, we also investigated whether oxygen was indeed essential for this process aiming to further validate the role of singlet oxygen. Interestingly, monitoring this process by fluorescence we observed a dramatic dependence on oxygen (ESI Fig. 15†), indicating singlet oxygen may indeed be the key reactive species. Nonetheless, addition of hydrogen peroxide can also promote the disruption of the acyl hydrazone linkage, but it requires quite large concentrations (100 mmol L^{-1} and higher) showing a slow kinetics as monitored by fluorescence (ESI Fig. S16†).

Isonicotinoyl radical production

The most accepted mechanism for the activation of isoniazid describes the formation of an isonicotinoyl radical as an intermediate, which eventually decays to isonicotinic acid or reacts with NAD(H) (nicotinamide adenine dinucleotide), producing the pharmacologically active adduct NAD-INH.[2] To validate the formation of this radical, EPR measurements were carried out using blue-light irradiation. **Ru-INH** was incubated with the

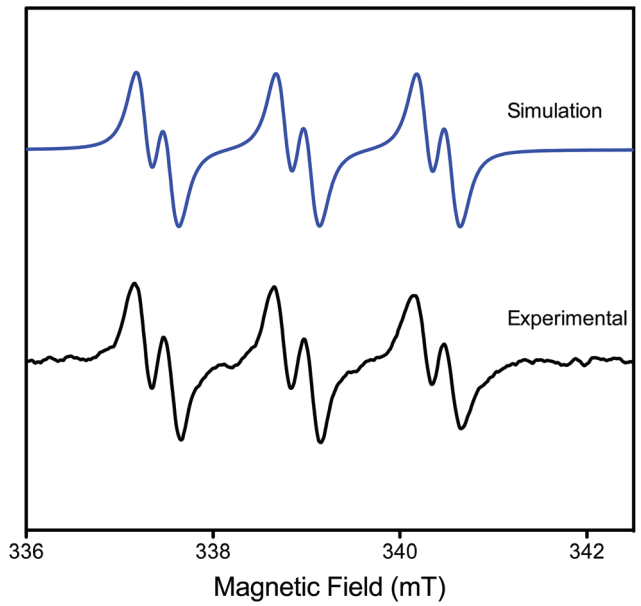

Fig. 4 EPR spectra of **Ru-INH** (5 mmol L^{-1}) in an aerated acetonitrile solution containing PBN (50 mmol L^{-1}), after *ca.* 20 h of blue-light irradiation (black) and spectral simulation of the isoniazid radical (blue). Measurement conditions: center field, 339 mT; sweep field, 10 mT; sweep time, 60 s; MW power, 20 mW; gain 2.0×10^3; modulation amplitude, 0.05 mT; modulation frequency, 100 kHz; time constant, 0.064 s; MW frequency, 9.50390 GHz. Spectral simulations were performed using the EasySpin program.[37]

spin trap PBN (*N-tert*-butyl-α-phenylnitrone) in acetonitrile, and irradiated with blue light for *ca.* 20 h at 23 °C. The EPR spectrum, shown in Fig. 6, presents a profile (a^N = 15.12 G and a^H = 2.66 G, g = 2.0059), consistent with a single radical, likely an isonicotinoyl species, as measured in aqueous solution (a^N = 14.3–16.5 G and a^H = 2.4–3.6) (Fig. 4).[6,8,44,45] Compared to the spectra previously reported for the isoniazid radical,[6,8] which presented hyperfine couplings of great symmetry, an asymmetry was observed here. Although this asymmetry had also been observed in aqueous systems from hepatocytes using isoniazid, in this work it is expected to be due to the acetonitrile medium, which exhibits a^H = 2.66 G and a linewidth of 0.149 mT.[44,45]

DNA cleavage

In addition to the formation of the isonicotinoyl radical, the isoniazid-conjugated ruthenium metal complex can photoproduce ROS species. We reasoned that this photoactivity might be important to enhance its anti-bacterial action. The DNA photodamage to pBR322 plasmid caused by **Ru-INH** in the dark and with blue-light irradiation was evaluated by electrophoretic assays. The gel analysis showed that **Ru-CHO** and **Ru-INH** were only able to cleave DNA upon blue-light irradiation (Fig. 5). The **Ru-INH** metal complex cleaved the plasmid DNA quite efficiently even at 5 μmol L^{-1}. The use of ROS scavenger species (sodium azide, for singlet oxygen; D-mannitol, for hydroxyl; catalase, for hydrogen peroxide; and superoxide dismutase, for superoxide ion) in this experiment highlighted the key role of singlet oxygen in this process, where sodium azide was the most efficient suppressor. This result agrees with the previous study with DPBF and APF probes.

Biological assays

To investigate the anti-bacterial activity of **Ru-INH**, we selected six different types of bacteria, including *Mycobacterium tuberculosis* and one multidrug resistant strain of Mtb. First, two Gram-positive and two Gram-negative pathogenic bacteria were tested with and without blue-light irradiation for 1 h

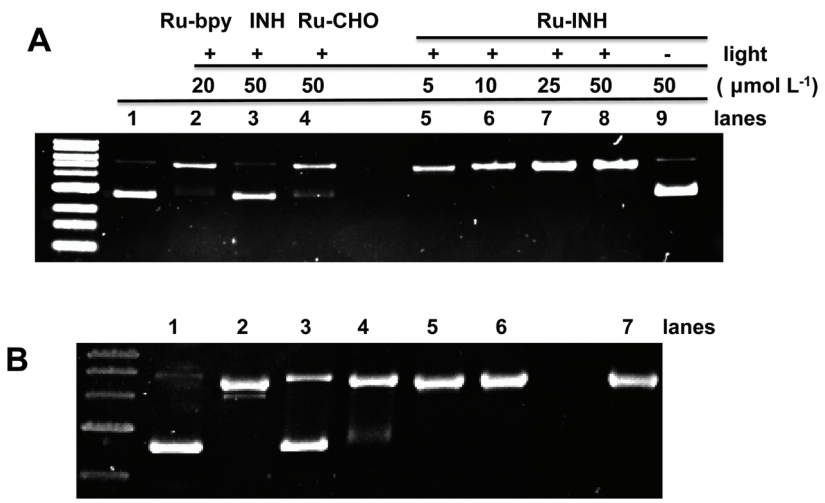

Fig. 5 DNA cleavage assay and mechanism. Panel A shows electrophoresis on agarose gel for the assay of plasmid DNA pBR322 with trisbipyridine ruthenium(II) (**Ru-bpy**, lane 2), isoniazid (**INH**, lane 3), bipyridine-aldehyde ruthenium(II) (**Ru-CHO**, lane 4), isoniazid-conjugated ruthenium(II) (**Ru-INH**, lanes 5 to 9); a linear DNA ladder is also shown (lane 1). Panel B shows the agarose gel assay for the blue-light irradiated isoniazid-conjugated metal complex alone (2), with the ROS scavengers sodium azide (3), D-mannitol (4), catalase (5) and superoxide dismutase (6); a control with trisbipyridine ruthenium(II) is in lane 7.

Table 1 Measurements of anti-bacterial activity

Compound	Bacterium	Blue LED	MIC, μmol L^{-1} (μg mL^{-1})	MBC, μmol L^{-1} (μg mL^{-1})
Ru-INH	*S. aureus*	ON	7.6 (7.8)	7.6 (7.8)
		OFF	n.d.	n.d.
	S. epidermidis	ON	30.6 (31.2)	30.6 (31.2)
		OFF	n.d.	n.d.
	P. aeruginosa	ON	61.2 (62.5)	61.2 (62.5)
		OFF	n.d.	n.d.
	E. coli	ON	122 (125)	122 (125)
		OFF	n.d.	n.d.
		—	6.1 (6.25)	—
Ru-CHO	*M. tuberculosis (H37Rv)*	—	>111 (100)	—
INH		—	2.8 (0.39)	—
Ru-INH	*M. tuberculosis (MDR, CDCT-16)*	—	>98 (100)	—
INH		—	>729 (100)	—

n.d. = not detected even at the highest concentration (125 μg mL^{-1}). Controls without ruthenium metal complexes and INH were prepared, also with and without blue light irradiation (max. 463 nm, 425 mW cm^{-2}).

(Table 1). Interestingly, only the light-irradiated samples showed anti-bacterial efficacy, while in the dark no measurable activity was noticed, indicating there is a tight control by blue light. Besides that, bacteria were also tested by applying only blue light without the metal complex, which has not caused any change in growth. The **Ru-INH** metal complex showed anti-bacterial activity towards Gram-positive as well as Gram-negative bacteria, with *S. aureus* exhibiting the best MIC (minimum inhibitory concentration) and MBC (minimum bactericidal concentration) values (7.6 μmol L^{-1}). Gram-negative bacteria showed lower susceptibility to this metal complex; similar results were obtained in our group's previous studies.[11,46,47] In addition to this, we were unable to measure any anti-bacterial activity for **Ru-CHO** or **INH** (up to 125 μg mL^{-1}) either with or without blue light irradiation.

We conducted a series of studies to evaluate the efficiency of **Ru-INH** against wild-type and multidrug-resistant *Mycobacterium tuberculosis* strains, using **Ru-CHO** and **INH** as references. Despite **Ru-CHO** being known as a good photogenerator of ROS, it did not show any anti-tuberculosis activity up to the maximum concentration employed (100 μg mL^{-1}, equivalent to 111 μmol L^{-1}). By contrast, **Ru-INH** showed promising activity, close to that observed for free isoniazid with the wild-type strain, but it was unable to kill the multidrug resistant strain (clinical isolate 16). It is important to note that these studies with *M. tuberculosis* were performed without blue-light irradiation due to technical restrictions, but we could not completely prevent light during the setup. We should also point out that the multidrug resistant strain contains several genetic alterations, including *katG* mutation (S315T), *inhA* promoter genotype (C(-15)T), and *rpoB* mutation (D516V). Therefore the **Ru-INH** metal complex has great anti-bacterial potential upon light stimulation (Table 1). This effect might not be only due to isoniazid activation, but possibly also, as indicated before, due to DNA degradation and other biological damage caused by singlet oxygen generation or even a direct effect of the metal complex. Nonetheless, the lowest MIC for *Mtb*, even without intentional light irradiation, is quite remarkable, taking into account that this bacterium has a highly selective cell wall, and makes this compound a promising agent.

We further performed cell viability assessments with mammalian cells, including normal murine fibroblast cells

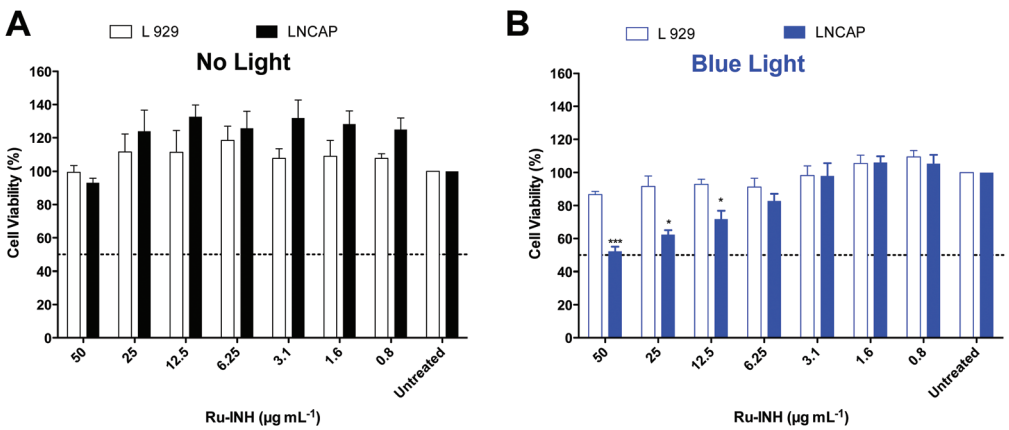

Fig. 6 Cell viability assay of L929 and LNCAP cells measured using MTS after 48 h of treatment with **Ru-INH** without (A) and with (B) blue-light irradiation (max. 463 nm, 425 mW cm^{-2}). *$P < 0.05$ and ***$P < 0.001$.

(NCTC-CL929) and human adenocarcinoma (lung A549, prostate LNCAP and breast MCF-7). These assays were conducted with and without blue-light irradiation. Previous screening had showed that **Ru-CHO** had no effect, with or without blue-light irradiation, on all the cell lines (data not shown). Moreover, **INH** and **Ru-INH** showed no significant cytotoxicity at up to 50 μg mL^{-1} without light irradiation (Fig. 6A and ESI Fig. S17†). However, with blue-light irradiation, we noticed an increase in the cytotoxicity of **Ru-INH** toward cell lines L929 and A549, but it was less effective toward MCF-7 cells and LNCAP (Fig. 6). Our results showed that **INH** alone had a cytotoxic effect against both normal and tumor cells (ESI Fig. S17 and S18†). On the other hand, when **INH** was conjugated to the ruthenium(II) metal complex, its antitumor effect became more selective, particularly in prostate adenocarcinoma (LNCAP). It is important to note that **Ru-INH** did not show toxic effects against normal cells (L929) when compared to cancer cells, as shown in Fig. 6. At 50, 25 and 12.5 μg mL^{-1} concentrations of **Ru-INH**, there was a reduction of 47.73 ± 2.82% (p = 0.0005), 37.60 ± 2.66% (p = 0.0132) and 28.20% ± 5.05% (p = 0.0246) in the cell population, respectively. Moreover, **Ru-INH** did not show any effect on the A549 and MCF-7 cell lines (data not shown). Our results suggest that **Ru-INH** reduces **INH** internalization by tumor cells. Probably, **INH** alone has a toxic effect at these dosages when coming into contact with the cell glicocalyx.[48] These results are exciting and support a good selectivity index for the potential use of **Ru-INH** also as an antitumor agent.

Conclusion

Altogether, we have evidence of the successful conjugation of isoniazid to a trisbipyridine-like ruthenium(II) metal complex yielding **Ru-INH**. This efficient conjugation reaction created an acyl hydrazone linkage that turned out to be essential for the photoactivation of isoniazid. Besides that, **Ru-INH** was shown to be stable in the dark and at a wide range of pH values. Only light selectively promoted linkage disruption. This photo-induced process was assigned to a singlet oxygen reaction produced *in situ* by the ruthenium(II) moiety, causing breakage of the acyl hydrazone group. As far as we know, this is the first time such a linkage has been disrupted by light. Despite the importance of this bonding disruption for producing an isonicotinoyl radical, a key species for anti-mycobacterial activity, the potential use of this linkage in other systems requiring activation (*e.g.* pyrazinamide) is also illustrated. Here, a proof-of-concept for a new light-activation strategy has been validated with isoniazid and a bipyridine ruthenium(II) metal complex, and the importance of using an acyl hydrazone linkage has been pointed out. This work goes beyond the photo-uncaging strategy: it also tackles key issues about drug activation, using a simple chemistry that opens great opportunities.

Although this phototherapy strategy is likely to be the most useful for superficial mycobacterial infections (*e.g. Mycobacterium ulcerans*), Gram-positive bacterial infections, or cancer, we should not be discouraged from applying it to more internal cases, as reported elsewhere.[49] Indeed, this could be considered particularly useful in hard-to-treat cases of extensively resistant strains of *M. tuberculosis*, for example, where the use of optical fibers devices for lung irradiation is not out of reach. Altogether, our results showed that a new and promising anti-microbial drug with low cytotoxicity was prepared employing a novel photoactivation strategy, which deserves further pharmacological studies.

Author contributions

EDN, ADV, LAB, EHT, ALA, MAV, LGNN, ACSG, AIBR, ORN, DZ, and EHSS designed the experiments. ADV, EHT, ALA, MAV, and LGNN conducted biological assays. EDN, ACSG, AIBR, ORN, and DZ carried out chemical and biochemical experiments. TFP carried out theoretical studies. EDN, ADV, LAB, EHT, ALA, MAV, LGNN, ACSG, ICND, AIBR, ORN, DZ, IMMC, LGFL, and EHSS analyzed and interpreted the data. EDN, LAB, EHT, ICND, ORN, DZ, TFP, IMMC, LGFL, and EHSS wrote the manuscript.

Conflicts of interest

There are no conflicts to declare.

Acknowledgements

We are indebted to Dr Felipe Diógenes Abreu for his initial assistance on this work, Geângela de Fátima Sousa Oliveira for support on anaerobic photochemical studies and Dr Marie-Alda Gilles-Gonzalez (UTSW) for English proofreading. We are thankful to the CAPES (PROEX 23038.000936/2018-46 and PRINT 88887.311905/2018-00), the CNPq (L. G. F. Lopes 303355/2018-2; E. H. S. Sousa 308383/2018-4, Universal 403866/2016-2; I. C. N. Diógenes 307078/2017-5; T. F. Paulo, Universal Universal 428741/2016-9), CONICYT (A. I. B. Romo #72170429), and FUNCAP (PRONEX PR2 0101-00030.01.00/15 SPU No.: 3265612/2015) for financial support. This work was also partially supported by the National Institute of Science and Technology on Tuberculosis (Decit/SCTIE/MS-MCT-CNPq FNDTC-CAPES-FAPERGS, grant number 421703/2017-2). We are also thankful to CENAPAD-UFC for allowing us to use the calculation facility for DFT and CENAUREM(UFC) for providing access to NMR equipment and also Dr Edilberto R. Silveira for his valuable assistance and discussions. This study was also financed in part by the Coordenação de Aperfeiçoamento de Pessoal de Nível Superior - Brasil (CAPES) - Finance Code 001.

Notes and references

1 WHO, *Global tuberculosis report*, World Health Organization, Geneva, 2018.
2 J. Laborde, C. Deraeve and V. Bernardes-Genisson, *ChemMedChem*, 2017, **12**, 1657–1676.

3 S. V. Ramaswamy, R. Reich, S. J. Dou, L. Jasperse, X. Pan, A. Wanger, T. Quitugua and E. A. Graviss, *Antimicrob. Agents Chemother.*, 2003, **47**, 1241–1250.
4 H. J. Marttila, H. Soini, E. Eerola, E. Vyshnevskaya, B. I. Vyshnevskiy, T. F. Otten, A. V. Vasilyef and M. K. Viljanen, *Antimicrob. Agents Chemother.*, 1998, **42**, 2443–2445.
5 E. H. S. Sousa, L. A. Basso, D. S. Santos, I. C. N. Diogenes, E. Longhinotti, L. G. D. Lopes and I. D. Moreira, *J. Biol. Inorg. Chem.*, 2012, **17**, 275–283.
6 J. Laborde, C. Deraeve, F. G. de Mesquita Vieira, A. Sournia-Saquet, L. Rechignat, A. D. Villela, B. L. Abbadi, F. S. Macchi, K. Pissinate, C. V. Bizarro, P. Machado, L. A. Basso, G. Pratviel, L. G. de Franca Lopes, E. H. S. Sousa and V. Bernardes-Genisson, *J. Inorg. Biochem.*, 2018, **179**, 71–81.
7 M. Nguyen, C. Claparols, J. Bernadou and B. Meunier, *ChemBioChem*, 2001, **2**, 877–883.
8 E. H. S. Sousa, F. G. D. Vieira, J. S. Butler, L. A. Basso, D. S. Santiago, I. C. N. Diogenes, L. G. D. Lopes and P. J. Sadler, *J. Inorg. Biochem.*, 2014, **140**, 236–244.
9 K. D. Mjos and C. Orvig, *Chem. Rev.*, 2014, **114**, 4540–4563.
10 N. P. E. Barry and P. J. Sadler, *Chem. Commun.*, 2013, **49**, 5106–5131.
11 F. D. Abreu, T. F. Paulo, M. H. Gehlen, R. A. Ando, L. G. F. Lopes, A. C. S. Gondim, M. A. Vasconcelos, E. H. Teixeira, E. H. S. Sousa and I. M. M. de Carvalho, *Inorg. Chem.*, 2017, **56**, 9084–9096.
12 J. J. Soldevila-Barreda and P. J. Sadler, *Curr. Opin. Chem. Biol.*, 2015, **25**, 172–183.
13 T. C. Johnstone, K. Suntharalingam and S. J. Lippard, *Chem. Rev.*, 2016, **116**, 3436–3486.
14 X. Wang, X. Wang, S. Jin, N. Muhammad and Z. Guo, *Chem. Rev.*, 2018, **119**, 1138–1192.
15 J. S. Oliveira, E. H. Sousa, L. A. Basso, M. Palaci, R. Dietze, D. S. Santos and I. S. Moreira, *Chem. Commun.*, 2004, 312–313, DOI: 10.1039/b313592f.
16 T. P. Gazzi, M. Rotta, A. D. Villela, V. Rodrigues, L. K. B. Martinelli, F. A. M. Sales, E. H. S. de Sousa, M. M. Campos, L. A. Basso, D. S. Santos and P. Machado, *J. Braz. Chem. Soc.*, 2017, **28**, 2028–2037.
17 E. H. Sousa, D. L. Pontes, I. C. Diogenes, L. G. Lopes, J. S. Oliveira, L. A. Basso, D. S. Santos and I. S. Moreira, *J. Inorg. Biochem.*, 2005, **99**, 368–375.
18 V. S. Rodrigues, A. dos Santos, A. J. Santos, C. Z. Schneider, J. B. Calixto, E. H. S. Sousa, L. G. D. Lopes, A. A. Souto, L. A. Basso, D. S. Santos and M. M. Campos, *Int. J. Antimicrob. Agents*, 2012, **40**, 182–185.
19 V. S. Rodrigues, A. A. dos Santos, A. D. Villela, J. M. Belardinelli, H. R. Morbidoni, L. A. Basso, M. M. Campos and D. S. Santos, *Int. J. Antimicrob. Agents*, 2014, **43**, 82–85.
20 V. S. Rodrigues, L. Cintra, P. Machado, A. Dadda, L. A. Basso, A. C. C. N. Mafra, A. H. Campos, M. M. Campos and D. S. Santos, *Regul. Toxicol. Pharmacol.*, 2017, **90**, 78–86.
21 V. S. Rodrigues, P. Machado, J. B. Calixto, J. M. Siqueira, E. L. Andrade, A. F. Bento, M. M. Campos, L. A. Basso and D. S. Santos, *Regul. Toxicol. Pharmacol.*, 2017, **86**, 11–17.
22 A. D. Dadda, V. S. Rodrigues, F. Carreno, G. O. Petersen, A. F. M. Pinto, P. F. Dalberto, N. D. M. Sperotto, K. Pissinate, C. V. Bizarro, P. Machado, M. M. Campos, T. Dalla Costa, D. S. Santos and L. A. Basso, *Eur. J. Pharm. Sci.*, 2018, **111**, 393–398.
23 B. L. Abbadi, A. D. Villela, V. S. Rodrigues-Junior, F. T. Subtil, P. F. Dalberto, A. P. S. Pinheiro, D. S. Santos, P. Machado, L. A. Basso and C. V. Bizarro, *Antimicrob. Agents Chemother.*, 2018 **62**(2), e02222-17.
24 N. A. Smith, P. Zhang, S. E. Greenough, M. D. Horbury, G. J. Clarkson, D. McFeely, A. Habtemariam, L. Salassa, V. G. Stavros, C. G. Dowson and P. J. Sadler, *Chem. Sci.*, 2017, **8**, 395–404.
25 R. N. Garner, C. G. Pierce, C. R. Reed and W. W. Brennessel, *Inorg. Chim. Acta*, 2017, **461**, 261–266.
26 I. Aguiar, A. Tavares, A. C. Roveda Jr., A. C. da Silva, L. B. Marino, E. O. Lopes, F. R. Pavan, L. G. Lopes and D. W. Franco, *Eur. J. Pharm. Sci.*, 2015, **70**, 45–54.
27 K. C. Hall, A. T. Franks, R. C. McAtee, M. S. Wang, V. I. Lu and K. J. Franz, *Photochem. Photobiol. Sci.*, 2017, **16**, 1604–1612.
28 X. Su and I. Aprahamian, *Chem. Soc. Rev.*, 2014, **43**, 1963–1981.
29 B. M. Peek, G. T. Ross, S. W. Edwards, G. J. Meyer, T. J. Meyer and B. W. Erickson, *Int. J. Pept. Protein Res.*, 1991, **38**, 114–123.
30 M. J. T. Frisch, G. W. Trucks, H. B. Schlegel, G. E. Scuseria, M. A. Robb, J. R. Cheeseman, G. Scalmani, V. Barone, B. Mennucci, G. A. Petersson, H. Nakatsuji, M. Caricato, X. Li, H. P. Hratchian, A. F. Izmaylov, J. Bloino, G. Zheng, J. L. Sonnenberg, M. Hada, M. Ehara, K. Toyota, R. Fukuda, J. Hasegawa, M. Ishida, T. Nakajima, Y. Honda, O. Kitao, H. Nakai, T. Vreven, J. A. Montgomery Jr., J. E. Peralta, F. Ogliaro, M. J. Bearpark, J. Heyd, E. N. Brothers, K. N. Kudin, V. N. Staroverov, R. Kobayashi, J. Normand, K. Raghavachari, A. P. Rendell, J. C. Burant, S. S. Iyengar, J. Tomasi, M. Cossi, N. Rega, N. J. Millam, M. Klene, J. E. Knox, J. B. Cross, V. Bakken, C. Adamo, J. Jaramillo, R. Gomperts, R. E. Stratmann, O. Yazyev, A. J. Austin, R. Cammi, C. Pomelli, J. W. Ochterski, R. L. Martin, K. Morokuma, V. G. Zakrzewski, G. A. Voth, P. Salvador, J. J. Dannenberg, S. Dapprich, A. D. Daniels, Ö. Farkas, J. B. Foresman, J. V. Ortiz, J. Cioslowski and D. J. Fox, Gaussian, Inc., Wallingford, CT, USA, 2009.
31 C. T. Lee, W. T. Yang and R. G. Parr, *Phys. Rev. B: Condens. Matter Mater. Phys.*, 1988, **37**, 785–789.
32 A. D. Becke, *J. Chem. Phys.*, 1993, 11623–11627.
33 P. J. Stephens, F. J. Devlin, C. F. Chabalowski and M. J. Frisch, *J. Phys. Chem.*, 1994, **98**, 11623–11627.
34 J. Tomasi, B. Mennucci and R. Cammi, *Chem. Rev.*, 2005, **105**, 2999–3093.
35 T. Lu and F. Chen, *J. Comput. Chem.*, 2012, **33**, 580–592.

36 N. M. O'Boyle, A. L. Tenderholt and K. M. Langner, *J. Comput. Chem.*, 2008, **29**, 839–845.
37 S. Stoll and A. Schweiger, *J. Magn. Reson.*, 2006, **178**, 42–55.
38 T. P. King, S. W. Zhao and T. Lam, *Biochemistry*, 1986, **25**, 5774–5779.
39 J. Kalia and R. T. Raines, *Angew. Chem., Int. Ed.*, 2008, 7523–7526.
40 I. Cvrtila, H. Fanlo-Virgos, G. Schaeffer, G. Monreal Santiago and S. Otto, *J. Am. Chem. Soc.*, 2017, **139**, 12459–12465.
41 M. Nguyen, A. Quemard, S. Broussy, J. Bernadou and B. Meunier, *Antimicrob. Agents Chemother.*, 2002, **46**, 2137–2144.
42 J. D. Knoll, B. A. Albani and C. Turro, *Acc. Chem. Res.*, 2015, **48**, 2280–2287.
43 C. Tanielian, C. Wolff and M. Esch, *J. Phys. Chem.*, 1996, **100**, 6555–6560.
44 E. Albano and A. Tomasi, *Biochem. Pharmacol.*, 1987, **36**, 2913–2920.
45 E. Albano, L. Goriagatti, P. Clot, A. Jannone and A. Tomasi, *Toxicol. Ind. Health*, 1993, **9**, 529–538.
46 A. de Sousa, A. Fernandes, I. Paz, N. Nascimento, J. Ellena, E. Sousa, L. Lopes and A. Holanda, *J. Braz. Chem. Soc.*, 2017, **28**, 2117–2129.
47 J. M. D. Carvalho, A. H. D. Batista, N. A. P. Nogueira, A. K. M. Holanda, J. R. de Sousa, D. Zampieri, M. J. B. Bezerra, F. S. Barreto, M. O. de Moraes, A. A. Batista, A. C. S. Gondim, T. D. F. Paulo, L. G. D. Lopes and E. H. S. Sousa, *New J. Chem.*, 2017, **41**, 13085–13095.
48 S. M. Cloonan, R. B. P. Elmes, M. Erby, S. A. Bright, F. E. Poynton, D. E. Nolan, S. J. Quinn, T. Gunnlaugsson and D. C. Williams, *J. Med. Chem.*, 2015, **58**, 4494–4505.
49 M. M. Lerch, M. J. Hansen, G. M. van Dam, W. Szymanski and B. L. Feringa, *Angew. Chem., Int. Ed.*, 2016, **55**, 10978–10999.

